DOI: 10.1002/stco.202100041

Dongsong Li, Markus Könemann, Michael Dölz, Sebastian Münstermann

REPRINT

A new method for the toughness assessment of mobile crane components based on damage mechanics

The characterization of toughness properties in standard Charpy or fracture mechanics tests calls for thickness requirements to be met. Therefore, the characterization of toughness properties is a problem for thin-walled structures. Replacing Charpy impact toughness testing by impact notch tensile testing can solve this problem. However, the toughness requirements are still expressed in terms of standard test results. Therefore, a framework is proposed here for translating these standard test requirements into impact notch tensile test requirements. The proposed framework relies on numerical simulations with a phenomenological damage mechanics model, which uses state-of-stress-dependent, strain-based criteria for the prediction of local damage and global fracture. This model takes the effects of non-proportional strain paths into account and applies different criteria for cleavage and ductile fracture in order to predict correctly the activation of cleavage and ductile fracture mechanisms in the corresponding numerical simulations.

Keywords toughness requirements; damage mechanics; mobile cranes; hollow sections

1 Introduction

Hollow sections are often used in industry to carry high mechanical loads. One critical point in the safety assessment for such structures is that standard toughness requirements have to be fulfilled. These days, toughness requirements can be derived quantitatively from fracture mechanics concepts. Once the requirements have been identified, empirical correlations to Charpy impact toughness values can be applied in the next step, so that, finally, fulfilling the requirements can be proved either by Charpy tests or by selecting materials with sufficient nominal Charpy toughness properties. Proving sufficient toughness becomes a problem if the material is too thin for the Charpy test. This becomes a problem for mobile crane structures, where ultrahigh-strength steel grades are used down to relatively thin gauges below 10 mm. Of course, in this specific case, sub-size Charpy tests can be performed, but the correlation to conventional Charpy test results is based on empirical knowledge only and might also overlook significant state-of-stress effects, especially when the thickness is well below the standard value of 10 mm. Therefore, a new technique is needed for the toughness characterization of structures made from thin-walled materials. Nevertheless, even if a new experimental approach exists to characterize the toughness of materials supplied in insufficient gauges, the problem persists that toughness requirements are typically expressed in terms of Charpy properties. So replacing the testing technique leads to the situation that toughness requirements that were defined as, for example, $T_{27\mathrm{J}}$ have to be translated into the parameters of the new test technique. This problem can be solved, however, by employing damage mechanics approaches. The aim of our research work is therefore the development of a new toughness testing setup suitable for thin-walled structures. Furthermore, a new concept is presented in this paper for translating the toughness requirements from the Charpy setup to the newly suggested one.

2 Conventional derivation of toughness requirements

The structural integrity assessment using fracture mechanics concepts has been successfully implemented for many applications. The principle of the fracture mechanics-based derivation of toughness requirements is the link between limits from non-destructive component testing, assumed cyclic crack propagation and the exclusion of brittle fracture even after cyclic crack propagation. Examples for the determination of toughness requirements based on this procedure can be found in [1, 2] and work as follows: After crack assumptions are established, fracture mechanics cyclic crack propagation calculations are performed to determine the crack size and geometry at the end of the intended service life or inspection and maintenance interval. For more details see [3–6]. Afterwards, the "Failure Assessment Diagram" is used for a limit state analysis in which the required material toughness is calculated for the design temperature. Subsequently, by applying the "Master Curve" concept developed by Wallin and now standardized in [7, 8], a required reference temperature T_{100} is obtained at which the structural material has a toughness $K_{\mathrm{IJ}} = 100 MPam^{\frac{1}{2}}$. In the optimum case the connection to the Charpy test is then made by empirically correlating the required temperature T_{100} with a temperature $T_{27\mathrm{J}}$ to be achieved in Charpy tests.

3 Derivation of toughness requirements using damage mechanics approaches

The fracture mechanics concept faces challenges in deriving toughness requirements for thin-walled structures and so damage mechanics approaches have been considered recently. Besson [9] divides models that explain damage

in a volumetric sense into two categories: coupled and uncoupled methods. Coupled models connect damage evolution to material flow behaviour, thus allowing damage-induced softening to be studied. Uncoupled techniques merely give fracture criteria. Similarly, damage evolution then has little effect on flow behaviour. The physical interpretation of damage allows for further subdivision of the coupled ductile damage mechanics models [10]. Micromechanical or porous plasticity models explain their damage development law in terms of void volume fractions, which are also incorporated into their yield potentials. The most common micromechanical technique is based on the Gurson-Tvergaard-Needleman (GTN) model [11–14]. However, there are also coupled ductile damage mechanics models that are constituted by phenomenological approaches. Their damage evolution equations are often based on the essential conditions for damage and fracture, which are stated as a weighted function of the equivalent plastic strain. Both experimental and computational research has revealed that stress triaxiality and Lode angle – two different variables that can be derived from the invariants of the stress tensor and the stress deviator – have a significant impact on the critical equivalent plastic strain to fracture, which is, by nature, a local parameter. One example is the Johnson-Cook model [15]. In this model the yield potential and the critical strain to ductile fracture are all affected by strain rate and temperature. However, according to the research of Bai and Wierzbicki, stress triaxiality and Lode angle should be taken into account to define the equivalent strain to ductile fracture [16]. The modified Bai-Wierzbicki model (MBW model) in its most recent formulation [17–20] derives the possible activation of the cleavage or ductile fracture mechanism based on local stress variables, where both stress- and strain-based criteria are used. To quantify these local parameters, the model is embedded in a numerical stress analysis based on FEM. A significant advantage of this local concept is the possibility for the quantitative evaluation of the existing stress state at any point in the structure due to the consideration of stress triaxiality and Lode angle.

4 Damage mechanics simulations

4.1 Modified Bai-Wierzbicki model

Both the Charpy test and the impact notch tensile test that will be suggested in section 5 of this article are subjected to the influences of stress state, temperature, strain rate and damage. All these influences have an effect on the material properties and failure behaviour. However, none of these influences are considered in the frequently used von Mises plasticity model. This leads to discrepancies between experimental and simulated test results. For this reason, an optimized yield potential was proposed by Bai and Wierzbicki, which includes the influences of the third invariant of the stress deviator J_3. Eq. (1) shows the formulation of this yield potential. First of all, it is noticeable that a comparison is still made with the von Mises equivalent stress σ_e. However, the yield stress σ_{yld} presented in Eq. (2) is now subjected to the influences of stress triaxiality and Lode angle. These two quantities are used to characterize the stress state in the deviatoric plane.

$$\Phi = \sigma_e - \sigma_{yld} \leq 0 \tag{1}$$

$$\sigma_{yld} = \bar{\sigma}\left(\bar{\varepsilon}^{pl}\right)\left[1 - c_\eta\left(\eta - \eta_0\right)\right]\left[\begin{matrix} c_\theta^s + \left(c_\theta^t - c_\theta^c\right) \\ \left(\gamma - \dfrac{\gamma^{m+1}}{m+1}\right) \end{matrix}\right] \tag{2}$$

Here, all c parameters as well as m are material constants, and $\bar{\sigma}(\bar{\varepsilon}^{pl})$ is the material's flow curve determined in reference tests with quasi-static boundary conditions [17]. The model can be used for both heavy plates and sheet metals, which is of particular importance for the investigations carried out here, where values are obtained from both round and flat specimens. Obviously, Bai and Wierzbicki have proposed a phenomenological model, which can be extended by including further influencing variables due to its mathematical flexibility. Here, additional terms are multiplicatively added to the yield stress, which allows thermal softening and strain rate hardening to be considered. Eq. (3) summarizes these influences on the yield stress. It is shown that all effects are multiplied by the basic yield curve description [18].

$$\sigma_{yld} = \bar{\sigma}\left(\bar{\varepsilon}^{pl}\right) * f\left(\eta, \bar{\theta}\right) * f\left(T\right) * f\left(\dot{\varepsilon}\right) \tag{3}$$

Thermal softening is described by the function $f(T)$ provided in Eq. (4). As the temperature increases, so this causes the yield stress to decrease. Likewise, dynamic strain hardening is expressed by a logarithmic function (Eq. (5)). In the simulation of complex loading conditions, an influence of all effects is to be expected [17].

$$f\left(T\right) = c_1^T * e^{-c_2^T * T} + c_3^T \tag{4}$$

$$f\left(\dot{\varepsilon}\right) = c_1^{\dot{\varepsilon}} * \ln\left(\dot{\varepsilon}^{pl}\right) + c_2^{\dot{\varepsilon}} \tag{5}$$

A pure plasticity model is not sufficient for simulating the tests introduced here. For this reason, a coupled damage mechanics model is used which, in addition to ductile damage, also allows the prediction of a cleavage fracture event. For this purpose, a damage variable is added to the yield potential introduced in Eq. (1). This yield potential is presented in Eq. (6).

$$\Phi = \sigma_e - \sigma_{yld}\left(1 - D\right) \leq 0 \tag{6}$$

The (1–D) term, which makes use of the damage variable D, is used to consider damage-induced softening effects. Consequently, damage evolution laws have to be provided. For this purpose, the model applies strain-based and stress-state-dependent criteria that distinguish between damage initiation and fracture. The framework was first described in [18] as a relatively simple approach for ductile fracture, but continuous developments over the last

eight years have resulted in a far more complex model formulation that allows features such as non-proportional strain paths or the concurrence between cleavage and ductile fracture mechanisms to be considered. The most recent model release for ductile fracture [19, 20] is therefore briefly described in the following. By relying on the invariants of the stress tensor (I_1, I_2, I_3) and the deviatoric stress tensor (J_1, J_2, J_3), it uses the stress triaxiality η (Eq. (7)) and the Lode angle parameter θ (Eqs. (8), (9)) to address the local state of stress:

$$\eta = \frac{I_1}{\sqrt{27 J_2}} \tag{7}$$

$$\theta = \frac{1}{3}\cos^{-1}\left(\sqrt{\frac{27}{4}} \cdot J_3 \cdot J_2^{-\frac{3}{2}}\right) \tag{8}$$

$$\bar{\theta} = 1 - 6\theta/\pi \tag{9}$$

In the model, it is assumed that under proportional strain paths, damage initiation is triggered when a critical equivalent plastic strain, known as the "damage initiation strain", has been reached. Since this critical value depends on the state of stress, it is expressed as the "damage initiation locus" (DIL), providing damage initiation strains $\bar{\varepsilon}^{\mathrm{p}}_{\mathrm{ddi}}\left(\eta,\bar{\theta}\right)$ as a function of stress triaxiality and Lode angle parameter (Eq. (10)):

$$\bar{\varepsilon}^{\mathrm{p}}_{\mathrm{ddi}}\left(\eta,\bar{\theta}\right) = \begin{pmatrix} D_1 \exp\left(-D_2\eta\right) - \\ D_3 \exp\left(-D_4\eta\right) \end{pmatrix} \cdot \bar{\theta}^2 + D_3 \exp\left(-D_4\eta\right) \tag{10}$$

In order to allow model predictions for non-proportional strain paths as well, the model makes use of an indicator for ductile damage initiation I_{ddi}. It ranges between 0 and 1, with 1 indicating the damage initiation event. The value of I_{ddi} (Eq. (11)) is calculated by integrating over the strain history according to the following approach:

$$I_{\mathrm{ddi}} = \int_0^{\bar{\varepsilon}^{\mathrm{p}}} \frac{1}{\bar{\varepsilon}^{\mathrm{p}}_{\mathrm{ddi}}\left(\eta_{\mathrm{average}},\bar{\theta}_{\mathrm{average}}\right)} d\bar{\varepsilon}^{\mathrm{p}} \tag{11}$$

The evolution of damage (or, more precisely, the rate of the damage variable $\dot{D}$) is afterwards described based on the understanding that a material point dissipates a characteristic amount of energy G_{f} (another material constant) between damage initiation and fracture. This is expressed in Eq. (12):

$$\dot{D} = \frac{\bar{\sigma}_{\mathrm{ddi}}}{G_{\mathrm{f}}} \dot{\bar{\varepsilon}}^{\mathrm{p}} \tag{12}$$

Finally, element deletion is applied when the equivalent plastic strain to fracture has been reached. Again, this is expressed based on an indicator concept relying on the stress-state-dependent "ductile fracture locus" (DFL), which is $\bar{\varepsilon}^{\mathrm{p}}_{\mathrm{df}}\left(\eta_{\mathrm{average}},\bar{\theta}_{\mathrm{average}}\right)$ in Eq. (13), thus considering non-proportional strain paths:

$$I_{\mathrm{df}} = \int_{\bar{\varepsilon}^{\mathrm{p}}_{\mathrm{ddi}}}^{\bar{\varepsilon}^{\mathrm{p}}} \frac{1}{\bar{\varepsilon}^{\mathrm{p}}_{\mathrm{df}}\left(\eta_{\mathrm{average}},\bar{\theta}_{\mathrm{average}}\right)} d\bar{\varepsilon}^{\mathrm{p}} \tag{13}$$

Other indicators are used to check whether a material point will not undergo ductile damage, but cleavage fracture instead [21, 22]. In general, the cleavage fracture part of the model assumes that cleavage fracture is a two-step process, with microdefect creation being step 1 and instable crack propagation step 2. The criterion for microdefect initiation is the strain-based, stress-state-dependent "microdefect initiation locus" $\bar{\varepsilon}^{\mathrm{p}}_{\mathrm{mdi}}\left(\eta,\bar{\theta}\right)$. This is expressed in Eq. (14):

$$\bar{\varepsilon}^{\mathrm{p}}_{\mathrm{mdi}}\left(\eta,\bar{\theta}\right) = \begin{pmatrix} F_1 \exp\left(-F_2\eta\right) - \\ F_3 \exp\left(-F_4\eta\right) \end{pmatrix} \cdot \bar{\theta}^2 + F_3 \exp\left(-F_4\eta\right) \tag{14}$$

Once this criterion has been fulfilled, the instable crack propagation for the special case of proportional strain paths is predicted by relying on the technical cleavage fracture stress σ_{c}. For the general case of non-proportional strain paths, the criterion is as follows in Eq. (15):

$$I_{\mathrm{mdi}} = \int_0^{\bar{\varepsilon}^{\mathrm{p}}} \frac{1}{\bar{\varepsilon}^{\mathrm{p}}_{\mathrm{mdi}}\left(\eta_{\mathrm{average}},\bar{\theta}_{\mathrm{average}}\right)} d\bar{\varepsilon}^{\mathrm{p}} \tag{15}$$

All these different indicators are finally merged into the following damage evolution law in Eq. (16):

$$D = \begin{cases} 0 & I_{\mathrm{mdi}} < 1 \\ 0 & I_{\mathrm{mdi}} \geq 1, I_{\mathrm{ddi}} < 1 \wedge \sigma_1 < \sigma_{\mathrm{c}} \\ 1 & I_{\mathrm{mdi}} \geq 1, I_{\mathrm{ddi}} < 1 \wedge \sigma_1 \geq \sigma_{\mathrm{c}} \\ 0 & I_{\mathrm{ddi}} < 1 \\ D_{\mathrm{cr}} \cdot I_{\mathrm{df}} & I_{\mathrm{ddi}} \geq 1 \wedge I_{\mathrm{df}} < 1 \\ 1 & I_{\mathrm{ddi}} \geq 1 \wedge I_{\mathrm{df}} \geq 1 \end{cases} \tag{16}$$

5 New impact toughness test for thin samples

A new measuring technique – the impact notch tensile test – is proposed for characterizing the impact toughness of a thin-walled material or thin-walled structure. A brief summary of how a conventional Charpy hammer had to be modified is given in the following.

A new hammer was installed in a Zwick pendulum impact tester (HIT50P), see Fig. 1. The maximum impact energy provided by this specific pendulum is 50 J. Furthermore, the specimen clamping mechanism had to be adjusted for this test procedure. A new yoke has been designed for use with relatively strong steel specimens, allowing friction and interlocked clamping of the sample. In addition, the sample container has been redesigned in such a way that the standard requirements for tempering samples can be fulfilled (in particular, the problem to be solved was that no more than 5 s may elapse between taking the samples out of the tempering system and the impact of the hammer). As a result, the sample holder is made up of two components that may be attached to the sample outside of the pendulum impact tester. The holder and sample are heated or cooled to the required test temperature, the sample placed in the pendulum impact tester and the test started immediately. A load cell in the

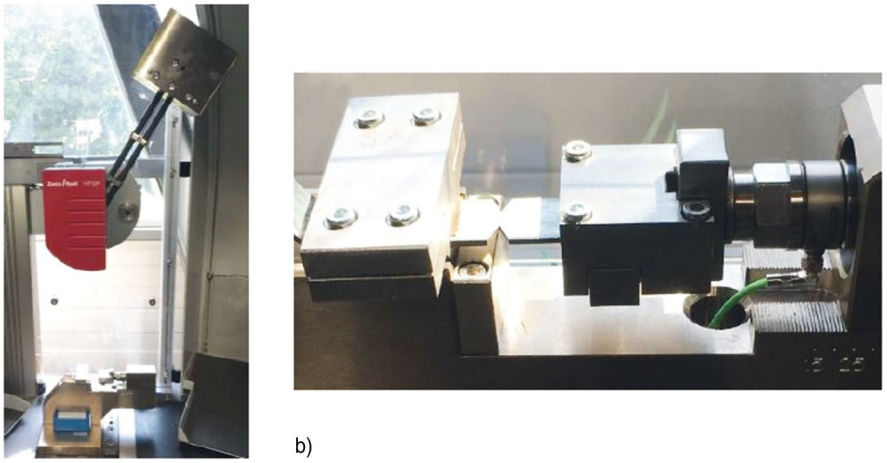

a) b)

Fig. 1 a) Impact pendulum with new hammer for tensile impact test, and b) clamping system with fixed specimen

area of the sample container is used to measure force. The force measurement is restricted to 10 kN due to the design of the machine. The deformation is recorded by an angle sensor situated in the centre of the pendulum.

Two buttons on the impact mechanism must be pressed to trigger the test. The hammer now drops and hits the specimen holder at a speed of 3800 mm/s, which is below the conventional hammer speed in 300 J Charpy hammers (5500 mm/s). The specimen is torn apart and the software is started. The sample is broken and an energy value is shown in the display. The software measures the force and displacement of the pendulum hammer during the test. The test itself takes only a few milliseconds, and only a few minutes are needed to prepare and clamp the specimen. About 10 to 20 minutes are needed to cool or heat the sample for different tempered samples. The test is therefore also suitable for checking the quality of the material during the production process.

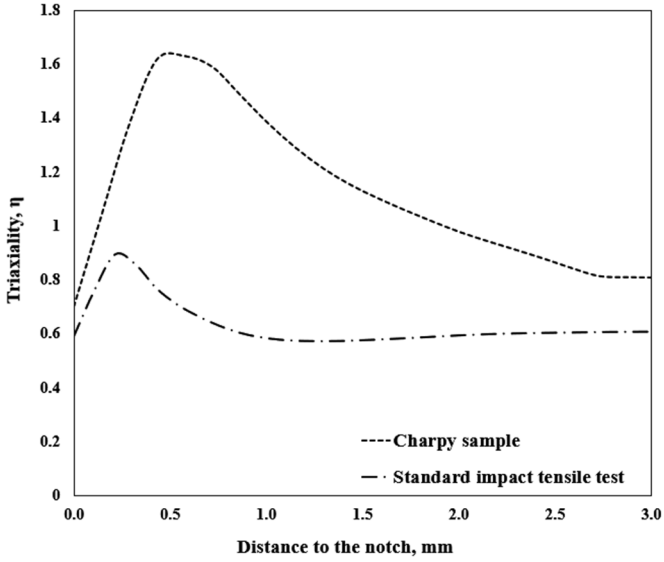

Fig. 2 Triaxiality comparison between Charpy sample and standard impact tensile sample

6 Correlation between Charpy test and impact notch tensile test

Since the toughness requirements are defined by the transition curve of the Charpy test, a correlation has to be made between the results from the Charpy test and the impact notch tensile test. Owing to the very different sample geometries of the Charpy test and the impact notch tensile test, a direct comparison of the transition curve is not feasible, because the stress triaxiality of these two samples differs significantly. In Fig. 2, triaxiality is plotted over the distance to the notch ground, revealing pronounced differences between the two geometries. These results are based on numerical simulations with the MBW model and they are valid for the situation in which the maximum force has been achieved during the test.

The cross-section of the Charpy sample is significantly larger than that of the impact notch tensile test sample, meaning that a direct comparison of the impact energies is not reasonable. Instead, the normalized energy is needed for a direct comparison. The normalized energy a_{VH} is defined by the fraction of the energy at different temperatures a and the energy at the upper shelf a_H (Eq. (17)).

$$a_{VH} = \frac{a}{a_H} * 100\% \tag{17}$$

In order to compare Charpy test results with impact notch tensile test results, a material had to be tested which fulfils two requirements: i) the material thickness is sufficient for manufacturing impact notch tensile test samples and standard Charpy samples (> 10 mm), ii) the maximum force during the impact notch tensile test remains below 10 kN. Both these requirements were fulfilled by a grade S355J2 structural steel, which was available in the stock of the authors' research institution. The material is 30 mm thick and has a ferritic-pearlitic microstructure. Its chemical composition is summarized in Tab. 1. Tensile tests were performed to characterize the material's strength properties, and Tab. 2 shows those properties.

Tab. 1 Chemical composition of S355J2 steel, mass contents in %

C	Si	Mn	P	S	Cr	Mo
0.143	0.49	1.42	0.012	< 0.001	0.04	< 0.01
Ni	**Al**	**Co**	**Cu**	**Nb**	**Ti**	**V**
0.03	0.037	< 0.01	0.03	0.03	< 0.01	< 0.01

Tab. 2 Strength properties of S355J2 steel

R_m [MPa]	$R_{p0.2}$ [MPa]	A_{40} [%]
526	365	35.9

Tab. 3 Energy and normalized energy of Charpy test for grade S355 steel

Temperature [°C]	Energy [J]	[%]
80	264.87	101.89
25	259.97	100.00
0	289.40	111.32
0	228.10	87.74
–20	220.73	84.91
–40	147.15	56.60
–40	157.00	60.39
–60	144.7	55.66
–80	19.62	7.55
–100	14.72	5.66
–120	14.72	5.66
–196	9.81	3.77

It is worth noting that this material selection is not really representative of the ultrahigh-strength steel used in mobile crane structures. Nevertheless, since the entire damage mechanics framework presented here is based on continuum mechanics, it can also be transferred to ultrahigh-strength steels. This holds particularly true because the physical mechanisms of ductile and cleavage fracture remain the same for both conventional structural steels and ultrahigh-strength steels. Tab. 3 shows the results of Charpy tests performed on a simple grade S355 structural steel . The results provided were afterwards normalized by relying on the upper shelf value a_H = 260J found at room temperature.

Afterwards, numerical simulations of impact notch tensile tests were performed in which the MBW model was applied. For this purpose, the MBW parameter set had to be calibrated. The conventional procedure for deriving these parameters has already been described in [18]. It is based on a curve-fitting approach that aims to achieve a good correlation between experiments and simulations for different sample geometries. It is important that the samples cover different characteristic stress states, which is typically achieved by precisely adjusting the sample geometries. Furthermore, temperatures have to be adjusted to make sure that parameters for both cleavage and ductile fracture can be identified. The experimental programme therefore covers tensile tests on notched dogbone samples, plane strain samples, shear samples and compression tests. All the notched samples cover different notch geometries. In addition, the entire programme is composed of experiments conducted at both room temperature (ductile fracture) and liquid nitrogen temperature (cleavage fracture).

For the material investigated, it turned out that a couple of simplifications were possible which reduced the number of parameters to be calibrated. Firstly, it was shown that an uncoupled description of ductile damage and fracture was possible because of late damage initiation and rapid damage evolution. This leads to the situation that $\bar{\varepsilon}^{p}_{ddi}\left(\eta_{average},\bar{\theta}_{average}\right) \cong \bar{\varepsilon}^{p}_{df}\left(\eta_{average},\bar{\theta}_{average}\right)$. Furthermore, it was observed that microdefects (tiny defects significantly smaller than the grain size, cavities at nonmetallic inclusions, broken particles) are already present in the material's microstructure, meaning that $\bar{\varepsilon}^{p}_{mdi}(\eta_{average},\theta_{average}) = 0$. Obviously, $\bar{\varepsilon}^{p}_{mdi}(\eta_{average},\theta_{average}) = 0$ is a conclusion that can be drawn for most structural steels containing usual amounts of impurities. On the other hand, a couple of modern steels, pipeline steels in particular, nowadays contain such small amounts of impurities that $\bar{\varepsilon}^{p}_{mdi}(\eta_{average},\theta_{average})$ is significantly larger than zero, which has very positive effects on the transition behaviours. The parameter set for the material investigated is summarized in Tab. 4.

Fig. 3 shows the dimensions of the standard geometry for the impact notch tensile test. These samples were modelled in Abaqus CAE. The tests were afterwards simulated

Tab. 4 MBW material parameters for S355

c_η	$c\frac{s}{\theta}$	$c\frac{t}{\theta}$	$c\frac{c}{\theta}$	m	D_1	D_2	D_3	D_4	G_f	D_{crit}
0.34	0.333	1.0	0.99	6.0	0.9	6.969	0.5815	4.646	7800	0.055
$c\frac{1}{T}$	$c\frac{2}{T}$	$c\frac{3}{T}$	$c\frac{1}{\dot{\varepsilon}}$	$c\frac{2}{\dot{\varepsilon}}$	$c\frac{3}{\dot{\varepsilon}}$	σ^*_f	F_1	F_2	F_3	F_4
1.82	0.01	0.9	0.0232	1.1069	0.0006	1399.0	0.25	3.502	1.5	4.979
σ_c										
1500										

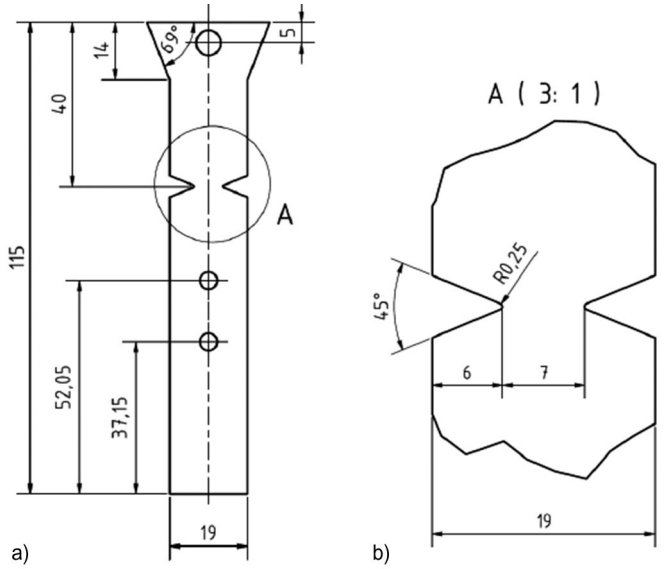

Fig. 3 Standard geometry of impact notch tensile test specimen: a) overall view and b) detail view of notch, 1.5 mm material thickness

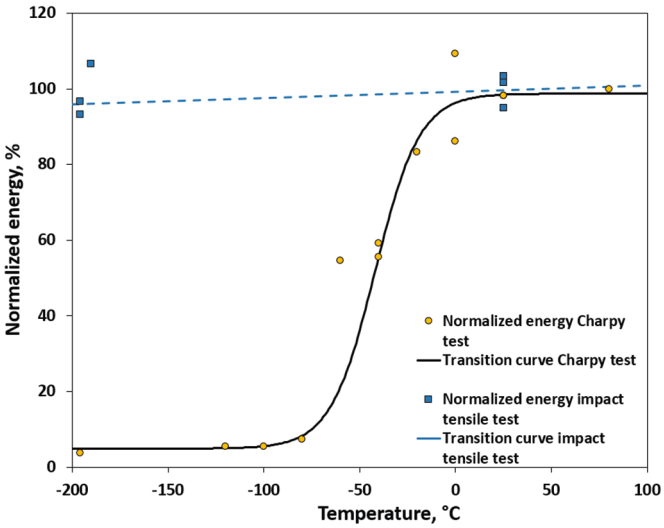

Fig. 4 Normalized energy from experimental Charpy test and impact notch tensile test with the support of FE simulation

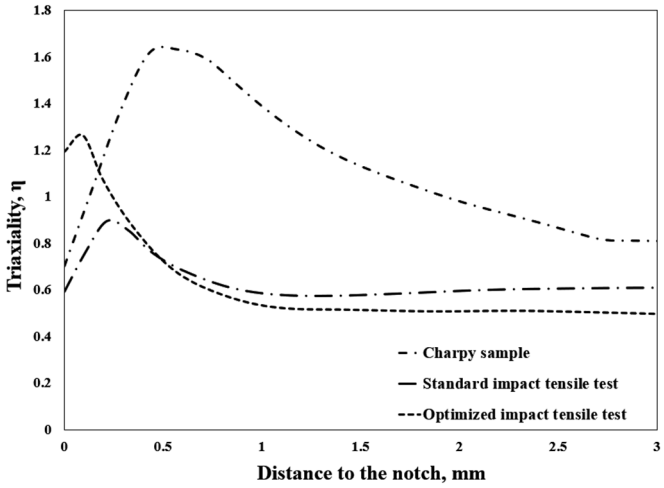

Fig. 5 Triaxiality comparison between Charpy sample, standard impact tensile sample and optimized impact tensile sample

with a VUMAT implementation of the MBW model. In this simulation, all members of the pendulum were modelled as rigid solids, and the initial temperature was systematically adjusted in order to be able to predict transition curves from impact notch tensile tests.

The normalized transition curves from Charpy test and impact notch tensile test simulations are shown in Fig. 4. However, it can be seen that the transition curve of the impact notch tensile test does not show the classical S-form transition behaviour within the temperature range tested here. Instead, it can be seen that the energy is almost constant over the entire temperature range investigated. This is because the triaxiality in the impact notch tensile test is so moderate that pronounced strain hardening is needed before cleavage fracture can be activated.

For a better correlation, an optimized impact tensile sample should therefore be developed with a triaxiality similar to that of the Charpy sample. For this purpose, a study was carried out to establish the dependence between impact notch tensile test sample geometry and the local stress triaxiality at the centre of the sample. To better understand this procedure, the following vocabulary is used: i) the "standard impact notch tensile test sample" is the geometry presented in Fig. 4, and ii) the "optimized impact notch tensile test sample" contains a sharper notch, compared with the standard sample, in order to approach the stress triaxiality of the Charpy sample.

The comparison of triaxiality between the Charpy sample, the standard impact notch tensile sample and the optimized impact notch tensile test sample is shown in Fig. 5. Again, this comparison was made for the loading situation in which the maximum force was achieved. According to the result of the comparison of the stress triaxiality, the optimized sample reaches higher stress triaxialities; however, it can be seen that the triaxiality of the optimized impact notch tensile test sample still does not reach the triaxiality of the Charpy sample. This is due to the following reasons: i) the thickness of the optimized impact tensile sample is still far different from the thickness of the Charpy sample, which therefore leads to the lower constraints in the transverse direction, and ii) bending stress is applied to the Charpy samples, whereas tensile stresses are applied to the notch impact tensile test samples. It is obviously impossible to achieve the same amount of stress triaxiality in both the impact notch tensile test and the Charpy test. Whether this discrepancy results in negligible or pronounced influences on the toughness test results will be explored in the following.

Besides the normalized scale of the energy, a new scale of temperature, the normalized temperature $T_{\mathrm{normalized}}$ (Eq. (18)), has also been defined, as this makes it easier to compare the impact notch tensile test and the Charpy test. The temperature axis is determined by a fraction of the test temperature and the temperature at half the upper shelf impact energy $0.5 * a_{\mathrm{H}}$. The transition curve can be calculated with the help of a tangent hyperbolic

Tab. 5 Transition temperature and T_0 values for Charpy Tests and impact tensile tests

$T_{a_{H/2}}$ Charpy	T_0 Charpy	$T_{a_{H/2}}$ impact tensile	T_0 impact tensile
–45°C	99.94 %	–40°C	100 %

function, which reproduces the classical S-shaped transition curves. This is expressed in Eq. (19):

$$T_{\text{normalized}} = \frac{T}{T_{\frac{a_H}{2}}} * 100 \tag{18}$$

$$a_{VH} = A + B * \tanh\left(\frac{\frac{T}{T_{a_{H/2}}} * 100 - T_0}{C}\right), A - B > 0 \tag{19}$$

Parameters A and B are constants needed to achieve a good fitting of the underlying experimental results. Furthermore, the ratio T_0 is used to shift the normalized transition curves left and right on the temperature axis. Please note that it is not a temperature, instead a temperature ratio that assumes 100 % when the transition temperature is reached. In the case of the transition curve of the notched bar impact test, the ratio was thus adjusted so that both types of test can be compared. The corresponding temperatures have to be entered in K. The values determined are shown in Tab. 5.

Ratio T_0 can therefore be understood as a measure of the effect of stress triaxiality on the transition curve. The ratio increases when the stress triaxiality in the impact notch tensile test sample is much lower than that in the Charpy sample, and it will be nearly 100 % when the stress triaxiality in both samples is almost identical.

Fig. 6 shows the correlation between the transition curves of the Charpy test and the impact notch tensile test. The optimized geometry of the impact notch tensile test sample was used in these investigations. A conventional S-shaped transition curve was predicted because the stress triaxiality increased significantly when the notch geometry was adjusted. It can be seen that $T_{a_{H/2}}$ for the Charpy test is located at –45 °C, whereas $T_{a_{H/2}}$ for the impact notch tensile test is located at –40 °C. From the comparison, it can be concluded that successful correlation of the two sample geometries is possible. With the support of the damage mechanics simulation, results of the impact notch tensile test can be translated accurately and successfully into results of the Charpy test. These findings are important because it proves that transition curves from impact notch tensile tests can be translated into conventional Charpy impact transition curves based on the parameter T_0, which is accessible to numerical damage mechanics simulations. Consequently, existing T_{27J} re-

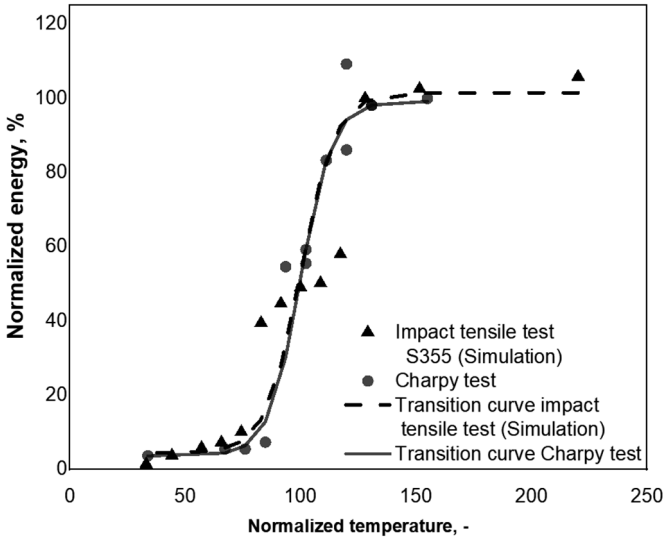

Fig. 6 Correlation between the transition curves of Charpy tests and impact notch tensile tests

quirements can be translated into corresponding requirements expressed in terms of impact notch tensile test results. And vice versa: toughness properties determined in impact notch tensile tests can be translated into Charpy impact toughness values even in cases where the material is too thin for producing standard Charpy samples.

7 Conclusions

A method has been proposed for the damage mechanics-based derivation of toughness requirements of thin-walled structures possibly made from ultrahigh-strength steels. So far, only a simple example has been discussed which creates a link between standard Charpy testing and the newly proposed impact notch tensile test. Obviously, this link has been proved to be valid for material grade S355 only, because the impact notch tensile test machine is not yet able to withstand forces higher than 10 kN. This raises questions concerning the transferability of the methodology to ultrahigh-strength steels. Owing to the phenomenological character of the continuum mechanics-based damage model used in this study, this transferability is ensured as long as the underlying mechanisms (dislocation slip-based plasticity, void-controlled ductile fracture, Griffith-type cleavage fracture) are still present, which is definitely the case for ultrahigh-strength structural steels. However, once the impact notch tensile test is transferred to a 300 J Charpy hammer, the entire methodology will be validated for ultrahigh-strength steels as well.

The findings of this work indicate that with the support of damage mechanics models for the simulation of impact notch tensile tests, it is possible to determine the toughness requirement of thin-walled hollow structures. This ensures the successful transfer of the results from the Charpy test and the impact notch tensile test, which is important for toughness characterization in the mobile crane industry. The following conclusions can be drawn:

- The impact notch tensile test is a new experimental technique for characterizing the toughness properties of structural materials.
- The effects of the stress state can lead to situations in which the microscopic mechanism is cleavage fracture, but high impact energy is still observed. This is based on the fact that pronounced strain hardening is required before the cleavage fracture stress can be reached.
- The framework presented allows conversion between Charpy impact toughness properties and impact notch tensile test properties. The main parameter to be considered is the temperature T_0, which shows a pronounced sensitivity to the stress triaxiality.
- In the future, the correlation should be established under the assumption of nominal properties. This will allow the toughness requirements to be defined in terms of new rules for material selection.

References

[1] Sedlacek, G.; Feldmann, M.; Kühn, B.; Tschickardt, D.; Höhler, S.; Müller, C.; Hensen, W.; Stranghöner, N.; Dahl, W.; Langenberg, P.; Münstermann, S.; Brozetti, J.; Raoul, J.; Pope, R.; Biljaard, F. (2008) *Material toughness and through thickness properties and other toughness oriented rules in EN 1993*: *Background document in support to the implementation, harmonization and further development of the Eurocodes*; Joint Report, Prepared under the JRC – ECCS.

[2] Stranghöner, N.; Sedlacek, G.; Stötzel, G.; Dahl, W.; Langenberg, P. (1998) *The choice of steel material for steel bridges to avoid brittle fracture*. Journal of Constructional Steel Research 1, No. 46, pp. 56–58.

[3] Sandström, R.; Langenberg, P.; Sieurin, H. (2004) *New brittle fracture model for the European pressure vessel standard*. International Journal of Pressure Vessels and Piping 81, No. 10–11, pp. 837–845.

[4] Sieurin, H.; Sandström, R.; Langenberg, P. (2003) *Crack detection performance and other assumptions for implementation in a model for avoidance of brittle fracture in pressure vessel steels*. Proc. of 29th MPa Seminar, Stuttgart, 9–10 Oct 2003.

[5] Pyttel, B.; Varfolomeyev, I.; Berger, C. (2007) *FKM-Richtlinie „Bruchmechanischer Festigkeitsnachweis für Maschinenbauteile“*. Mat.-wiss. u. Werkstofftech. 38, No. 5, pp. 387–397.

[6] British Standard BS 7910:2019 (2019) *Guide to methods for assessing the acceptability of flaws in metallic structures*.

[7] Wallin, K. (1991) *Statistical modeling of fracture in the ductile-to-brittle transition range*. Defect Assessment in Components, Fundamentals and Applications. Mechanical Engineering Publications, pp. 415–445.

[8] ASME 1921-02 (2002) *Standard test method for determination of reference temperature T0 for ferritic steels in the transition range*. Annual Book of ASTM Standards ASTM, Philadelphia.

[9] Besson, J. (2009) *Continuum models of ductile fracture*. International Journal of Damage Mechnics 19. No. 1, pp. 3–52.

[10] Münstermann, S.; Lian, J.; Bleck, W. (2012) *Design of damage tolerance in high-strength steels* in: Int J Mat Res 103, pp. 755–764.

[11] Gurson, A. L. (1977) *Continuum Theory of Ductile Rupture by Void Nucleation and Growth: Part I – Yield Criteria and Flow Rules for Porous Ductile Media*. J. Eng. Mater. Technol. 99, No. 1, pp. 2–15.

[12] Tvergaard, V. (1981) *Influence of voids on shear band instabilities under plane-strain conditions*. Int J Fracture 17, pp. 389–407.

[13] Tvergaard, V. (1982) *On localization in ductile materials containing spherical voids*.: Int J Fracture 18, pp. 237–252.

[14] Needlemann, A.; Tvergaard, V. (1995) *Analysis of a brittle-ductile transition under dynamic shear loading*. International Journal of Solids and Structures 32, No. 17–18, pp. 2571–2590.

[15] Johnson, G.; Cook, W. (1985) *Fracture characteristics of three metals subjected to various strains, strain rates, temperatures and pressures*. Eng Fract Mech 21, pp. 31–48.

[16] Bai, Y.; Wierzbicki, T. (2008) *A new model of metal plasticity and fracture with pressure and Lode dependence*. International Journal of Plasticity 24, pp. 1071–1096.

[17] Wu, B.; Vajragupta, N.; Lian, J.; Hangen, U.; Wechsuwanmanee, P.; Münstermann, S. (2017) *Prediction of plasticity and damage initiation behaviour of C45E+ N steel by micromechanical modelling*. Materials & Design 121, pp. 154–166,

[18] Lian, J.; Sharaf, M.; Archie, F.; Münstermann, S. (2012) *A hybrid approach for modelling of plasticity and failure behavior of advanced high-strength steel sheets*. International Journal of Damage Mechanics 22, No. 2, pp. 188–218.

[19] Pütz, F.; Shen, F.; Könemann, M.; Münstermann, S. (2020) *The differences of damage initiation and accumulation of DP steels: a numerical and experimental analysis*. International Journal of Fracture 226, pp. 1–15.

[20] Liu, W.; Lian, J.; Münstermann, S.; Zeng, C.; Fang, X. (2020) *Prediction of crack formation in the progressive folding of square tubes during dynamic axial crushing*. International Journal of Mechanical Sciences 176, article No. 105534.

[21] He, J.; Lian, J.; Golisch, G.; Jie, X.; Münstermann, S. (2017) *A generalized Orowan model for cleavage fracture*. Engineering fracture mechanics 186, pp. 105–118.

[22] He, J.; Lian, J.; Golsich, G.; He, A.; Di, Y.; Münstermann, S. (2017) *Investigation on micromechanism and stress state effects on cleavage fracture of ferritic-pearlitic steel at-196 degrees C*. Materials Science and Engineering A – Structural Material Properties, Microstructure and Processing 686, pp. 134–141.

Authors
Dongsong Li, M.Sc. (corresponding author)
dongsong.li@iehk.rwth-aachen.de
RWTH Aachen University
Academic and Research Department Integrity of Materials and Structures
Intzestr.1
52072 Aachen, Germany

Dr.-Ing. Markus Könemann
markus.koenemann@iehk.rwth-aachen.de
RWTH Aachen University
Academic and Research Department Integrity of Materials and Structures
Intzestr.1
52072 Aachen, Germany

Dr.-Ing. Michael Dölz
michael.doelz@iehk.rwth-aachen.de
RWTH Aachen University
Academic and Research Department Integrity of Materials and Structures
Intzestr.1
52072 Aachen, Germany

Dr.-Ing., Universitätsprofessor Sebastian Münstermann
sebastian.muenstermann@iehk.rwth-aachen.de
RWTH Aachen University
Academic and Research Department Integrity of Materials and Structures
Intzestr.1
52072 Aachen, Germany

How to Cite this Paper

Li, D.; Könemann, M.; Dölz, M.; Münstermann, S. (2022) *A new method for the toughness assessment of mobile crane components based on damage mechanics.* Steel Construction 15, Hollow Sections, pp. 69–77. https://doi.org/10.1002/stco.202100041

This paper has been peer reviewed. Submitted: 11. November 2021; accepted: 14. February 2022.